ACS OMEGA

Article

Cite This: ACS Omega 2017, 2, 8751−8759

Scalable Chitosan-Graphene Oxide Membranes: The Effect of GO Size on Properties and Cross-Flow Filtration Performance

Mojtaba Abolhassani,[†] Chris S. Griggs,[‡] Luke A. Gurtowski,[‡] Jose A. Mattei-Sosa,[‡] Michelle Nevins,[‡,§] Victor F. Medina,[‡] Timothy A. Morgan,[∥] and Lauren F. Greenlee*[,†]

[†]Ralph E. Martin Department of Chemical Engineering, 3202 Bell Engineering Center, University of Arkansas, Fayetteville, Arkansas 72701, United States

[‡]U.S. Army Engineer Research Development Center, 3909 Halls Ferry Road, Vicksburg, Mississippi 39180, United States

[§]State University of New York at Stony Brook, Stony Brook, New York 11794, United States

[∥]Institute for Nanoscience and Engineering, University of Arkansas, 731 W Dickson Street, Fayetteville, Arkansas 72701, United States

Supporting Information

ABSTRACT: Chitosan (CS)-graphene oxide (GO) composite films were fabricated, characterized, and evaluated as pressure-driven water filtration membranes. GO particles were incorporated into a chitosan polymer solution to form a suspension that was cast as a membrane via evaporative phase inversion allowing for scale-up for cross-flow testing conditions. Morphology and composition results for nano and granular GO in the CS matrix indicate that the particle size of GO impacts the internal membrane morphology as well as the structural order and the chemical composition. Performance of the membranes was evaluated with cationic and anionic organic probe molecules and revealed charge-dependent mechanisms of dye removal. The CSGO membranes had rejections of at least 95% for cationic methylene blue with mass balances obtained from measurements of the feed, concentrate, and permeate. This result suggests the dominant mechanism of removal is physical rejection for both GO particle sizes. For anionic methyl orange, the results indicate sorption as the dominant mechanism of removal, and performance is dependent on both GO particle size and time, with micrometer-scale GO removing 68−99% and nanometer-scale GO showing modest removal of 29−64%. The pure water flux for CSGO composite membranes ranged from 2−4.5 L/m^2 h at a transmembrane pressure of 344 kPa (3.44 bar), with pure water permeance ranging from 5.8×10^{-3} to 0.01 L/m^2 h kPa (0.58−1.3 L/m^2 h bar). Based on the 41 μm membrane thickness obtained from microscopy, the hydraulic permeability ranged from 0.24−0.54 L μm/m^2 h kPa (24.4−54.1 L μm/m^2 h bar).

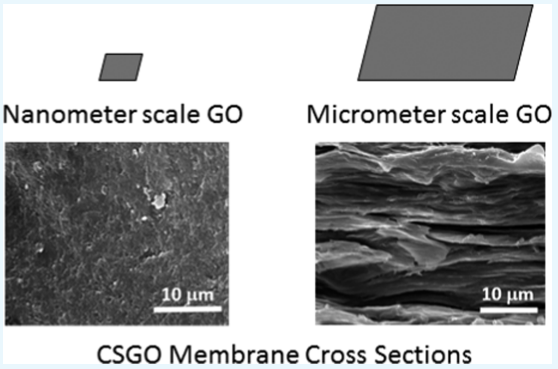

1. INTRODUCTION

Membrane filtration is a cost-effective water treatment method that provides excellent removal for a wide range of aqueous contaminants with a relatively long lifetime and high product recovery.[1] Novel nanomaterials provide an opportunity to develop membranes in the nanofiltration regime that can address the removal of contaminants not typically removed by microfiltration or ultrafiltration.[2,3] Polymeric membranes are the most favorable candidates for nanofiltration membranes due to advantageous thermal and chemical stability.[4] Thermal and chemical stability in a wide range of pH are observed for different polymeric membranes, including poly(ether sulfone) (PES),[5] poly(vinylidene difluoride) (PVDF),[6,7] polypyrrole (PPy),[8] poly(*m*-phenylene isophthalamide) (PMIA),[9] polyamide (PA),[10] and polysulfone (PSF).[4] However, membrane fouling, low flux, and low hydrophilicity are challenges that remain.[11,12] Further, most polymers are derived from petroleum and thus represent a fossil-fuel-based resource that presents opportunities for more environmentally sustainable alternatives.

Chitosan (CS) is a polymer and a derivative of chitin, which is the second most abundant naturally occurring biopolymer on Earth. Due to its biocompatibility, biodegradability, low toxicity, and antibacterial and hemostatic properties, CS is a promising low-cost, renewable alternative to petroleum-based synthetic polymers. Moreover, CS contains amino and hydroxyl functional groups, which make CS hydrophilic. However, the weak mechanical properties and the solubility of CS in acidic aqueous environments are two critical challenges.[13,14] Modification methods, including cross-linking strategies and the use of mechanical reinforcement agents, can result in a more robust membrane material that can overcome these drawbacks.[15−17]

Received: August 29, 2017
Accepted: November 22, 2017
Published: December 7, 2017

DOI: 10.1021/acsomega.7b01266
ACS Omega 2017, 2, 8751−8759

Carbon nanotubes and graphene as carbon-based nanofillers are not ideal due to toxicity, hydrophobic properties, and agglomeration. Graphene oxide (GO) is produced by chemical modification of graphene, where oxidation causes the addition of hydroxyl, carboxyl, and epoxide functional groups to the basal planes and edges of the graphene sheets.[18] These functional groups make GO amphiphilic with hydrophobic basal planes and hydrophilic edges.[19,20] GO also has a high surface area, and studies have shown that it is effective for adsorptive removal of heavy metal ions and cationic dyes from water.[21,22] The oxidative surface modification of GO also enables its use as a dispersible nanofiller for water filtration membranes due to the strong interactions between hydrophilic polymer functional groups and GO.[14,23] The addition of GO to polymeric membranes comprised of PA,[10] PES,[5] PMIA,[9] PSF,[24] and PVDF[6,7] resulted in decreased fouling, as well as increased hydrophilicity and flux. The addition of GO to a polymer matrix can also improve the thermal stability and mechanical strength of the membrane[5] and results in demonstrated increases in salt rejection for PA,[10] protein rejection for PES,[5] arsenic rejection for PSF,[24] and dye rejection for PMIA membranes.[9]

Chitosan-graphene oxide (CSGO) nanocomposites have been investigated for drug delivery, bone tissue engineering, and water treatment.[25,26] Strong hydrogen bonds and electrostatic attraction between negatively charged GO sheets and positively charged polysaccharide groups in CS make CSGO a stable and biocompatible nanocomposite with excellent mechanical and thermal properties.[14,27−29] Therefore, CSGO composites can potentially be used for hydrostatic pressure-based water filtration applications, where mechanical stability is necessary.[30] However, the application of CSGO as a membrane or film has been limited to tissue engineering,[31] drug delivery,[27] sensors,[32,33] and similar applications.[30] In water treatment applications, CSGO nanocomposites have primarily been used as an adsorbent to remove contaminants such as chromium,[34] copper ions,[35] other metal ions,[25,36] and dye molecules[14] from water. Earlier reports on GO membranes have been limited to small experimental volumes and short durations, which are not representative of real-world membrane operation.[37] To our knowledge, no significant work has explored CSGO membranes for pressure-driven water filtration.

In this study, we present results on the morphology, composition, structure, and water treatment performance of a unique set of CSGO composite membranes where two sizes of GO particles, granular GO (0.3−0.7 μm in diameter) and nanoscale GO (90 nm in diameter), are evaluated at a CS/GO ratio of 5:1 w/w and are compared to GO- and CS-only membranes.

2. RESULTS AND DISCUSSION

2.1. Morphology of CSGO Membranes. GO, CS/0, and CSGO membranes were first characterized by scanning electron microscopy (SEM) to assess the morphology and distribution of GO particles in the CS matrix (Figure 1). CSGO membranes that contain granular and nanoscale GO are designated as DG-CSGO and DN-CSGO, respectively. The GO membrane, GO-free CS/0 membrane, and DG-CSGO membrane in Figure 1a−c, respectively, have a smooth and homogeneous top surface. However, the DN-CSGO membrane's top surface, shown in Figure 1d, has a rough top surface morphology, where the structures observed are due to the presence of nanoscale GO in the CS matrix. Because the top

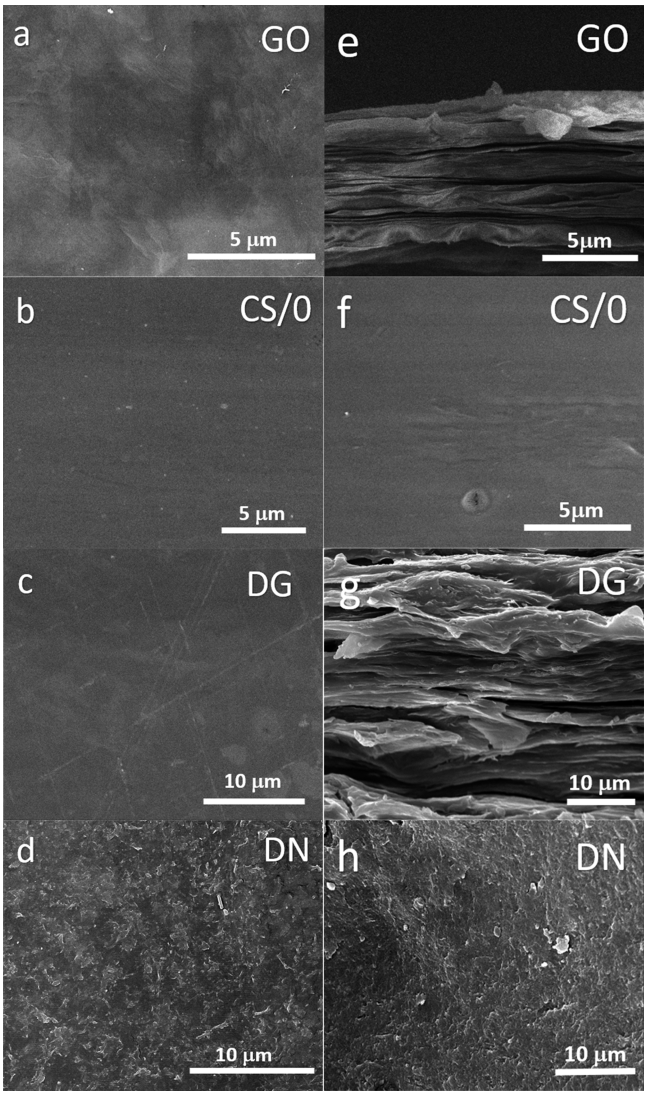

Figure 1. SEM images of the top surface of (a) GO, (b) CS/0, (c) DG-CSGO, and (d) DN-CSGO membranes. SEM cross-sectional images of (e) GO, (f) CS/0, (g) DG-CSGO, and (h) DN-CSGO membranes. The different 5 and 10 μm magnifications were chosen to highlight the detail and layering arrangement of the membranes with appropriate comparison.

surface morphology of the DN-CSGO membrane is unlike that of either the GO membrane or the CS/0 membrane, it is difficult to evaluate whether the CS or the GO controls the top surface morphology. However, the different morphology observed in the DN-CSGO membrane suggests that the presence of GO can cause a change in morphology, as compared to GO-free CS/0.

The cross-sectional images in Figure 1e−h further support this conclusion, as the cross-sectional membrane morphology for GO (Figure 1e) and DG-CSGO (Figure 1g) are quite similar (layered structure of stacked sheets).[38,39] In comparison, the cross-sectional membrane morphology for DN-CSGO membrane resulted in a nacrelike structure (Figure 1h), which suggests the GO sheets wrapped with CS polymer.[17] Neither of the two CSGO membrane cross-sectional morphologies resemble the CS/0 cross-sectional morphology, which is smooth and homogeneous, similar to the CS/0 top surface morphology. Overall, it appears that the incorporation of GO

DOI: 10.1021/acsomega.7b01266
ACS Omega 2017, 2, 8751−8759

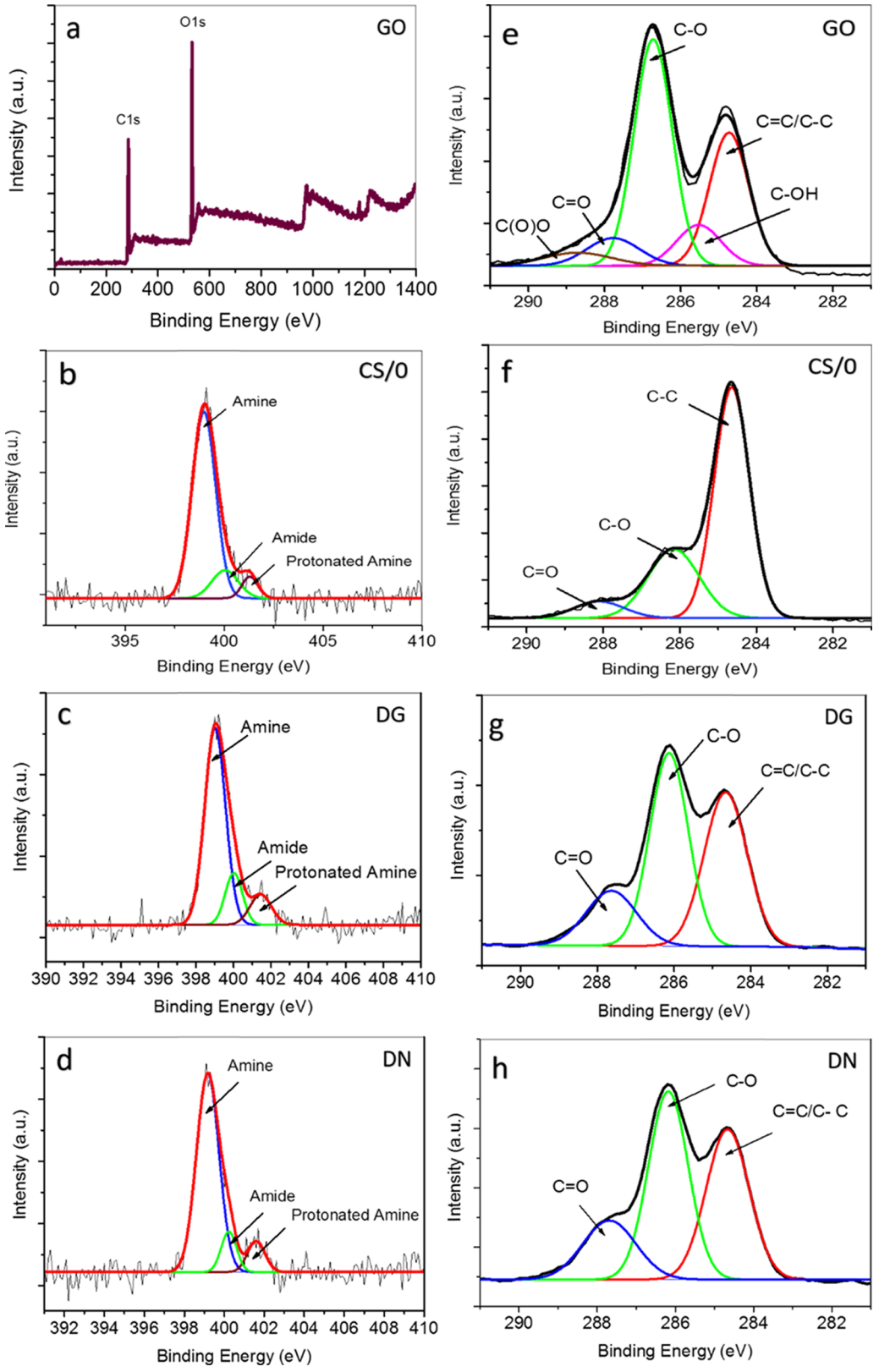

Figure 2. XPS N 1s spectra of (a) GO, (b) CS/0, (c) DG-CSGO, and (d) DN-CSGO membranes. C 1s spectra of (e) GO, (f) CS/0, (g) DG-CSGO, and (h) DN-CSGO membranes.

into a CS membrane can cause significant changes in the top surface and cross-sectional morphology, where GO appears to control the resulting morphology, rather than CS. Furthermore, the size of the GO clearly has an impact on the resulting membrane morphology. Membrane thickness was determined to be 8.2, 52.5, 41.3, and 39.4 μm for GO, CS/0, DG-CSGO, and DN-CSGO, respectively, using the SEM cross-sectional images (Supporting Information, Figure S2a–d).

DOI: 10.1021/acsomega.7b01266
ACS Omega 2017, 2, 8751–8759

2.2. Chemical Composition of CSGO Composite Membranes. To assess the chemical composition of each membrane, all of the membrane samples were characterized by X-ray photoelectron spectroscopy (XPS) (Figure 2a–h). The initial survey scans were taken between 0 and 1400 eV binding energy for CS, GO, and CSGO films (survey scan of GO shown in Figure 2a). The XPS survey scans were subsequently followed by detailed scans for carbon (C) (275–295 eV) for all of the samples (Figure 2e–h) and nitrogen (N) (390–410 eV) for the CSGO membranes and the CS/0 membrane (Figure 2c–e). In addition, a detailed survey scan for Al (70–80 eV) was performed for the GO membrane (Supporting Information, Figure S3). The C 1s GO spectrum was analyzed for five types of C atom, where C is part of a covalent bond with another element (C, hydrogen (H), or oxygen (O)). Peaks assigned at 285.6, 286.8, 288, and 289.4 eV correspond to C–OH, C–O, C═O, and C(O)O groups, respectively.[40] In addition, the first peak at 284.8 eV is a combination of C–C and C═C bonds.[41] The C–O peak represents the epoxide groups typically found on the surface of GO.[40] Hydroxyl (C–OH), carboxyl (C(O)O), and carbonyl (C═O) peaks are also observed and expected on the oxidized surface of GO. The dominant oxidized group is the epoxide group, and a significant C═C peak is also observed, illustrating the graphene-based honeycomb of carbon rings that is the backbone structure of GO. However, the C–C and C═C peaks are close to each other, and a smaller C═C peak is likely to be obscured by the large C–C peak, preventing a full analysis of C–C versus C═C bonding with XPS.

The C 1s XPS spectrum of the CS/0 membrane indicates the presence of C–C, C–O, and C═O groups at 284.8, 286.9, and 287.9 eV, respectively, whereas the XPS results for both CSGO membranes indicate the presence of C═C/C–C, C–O, and C═O groups at 284.8, 286.9, and 287.9 eV, respectively.[42] In comparison to the CS/0 membrane, the spectra for CSGO membranes result in a wider peak at around 284.7 eV, indicating the presence of C═C, along with the characteristic peak at 284.8 eV for the C–C group. Further, the intensity of the peaks for C–O and C═O are larger due to the contribution of GO.[42]

The initial survey scans for the GO membrane resulted in no observed peaks in the N 1s region (Figure 2a), as was expected, as GO by itself contains no nitrogen groups. The N 1s spectrum for the CS/0 membrane (Figure 2b) resulted in three peaks that can be correlated to the amine ($C-NH_2$), amide (C–NHC═O), and protonated amine species ($C-NH_3^+$) at 399.4 (86.34%), 400.5 (9.56%), and 401.7 eV (4.10%), respectively. Results for the N 1s XPS spectra are shown in Figure 2c,d for the DG-CSGO and DN-CSGO membranes, with no obvious difference between the two CSGO membranes. However, there are shifts in the peak intensities and related relative contributions to the N group speciation in CSGO membranes, as compared to the GO-free CS/0 membrane. The results, summarized in Table 1, indicate a reduction in the amine group contribution from 86.34% for the CS/0 membrane to 80.68 and 83.50% for DG-CSGO and DN-CSGO membranes, respectively. Moreover, an increase in protonated amine species from 4.10% for the CS/0 membrane to 6.68 and 6.64% for DG-CSGO and DN-CSGO membranes, respectively, is observed. The amide species contribution also increased for DG-CSGO (12.64%) and, to a lesser extent, for DN-CSGO (9.86%) membranes, as compared to the CS/0 membrane (9.56%). The reduction in amine and increase in protonated amine and amide species is likely connected to the electrostatic and hydrogen-bonding interactions that form between the N-based groups in CS and the oxidized functional groups on the GO surface.[43] In particular, both hydroxyl and carboxyl groups on the GO surface could facilitate the formation of protonated amine groups between CS and GO, whereas the carbonyl and epoxide groups could potentially participate in the formation of amide linkages through either electrostatic interactions or covalent bonds.

Table 1. Summary of N 1s and C 1s Peak Analysis for All Four Membranes

membrane	N1[a] (%) (399.4)	N2[a] (%) (400.5)	N3[a] (%) (401.7)	C/O ratio
GO				2
CS/0	86.34	9.56	4.10	5
DG-CSGO	80.68	12.64	6.68	2.2
DN-CSGO	83.50	9.86	6.64	2.3

[a]N1, N2, and N3 are related to amine, amide, and protonated amine species, respectively.

When the results for the N group speciation between the DG-CSGO membrane and the DN-CSGO membrane are compared, the granular GO particles appear to have a larger effect on speciation than the nanoscale GO particles. This result suggests that the size of the GO particles is not only important for controlling membrane morphology, as shown in Figure 1, but is also important for controlling the interactions between the CS polymer and the GO particles in the composite membrane. In this study, the GO powder of each particle size was added at the same mass concentration to the CS solution to make the membranes. For the same mass, the larger, granular GO would have a larger ratio of top and bottom surface area to basal plane edges, as compared to the nanoscale GO, which would have more edge surface area on a per mass basis, given the smaller particle size. However, previous studies suggest that oxygen-containing functional groups are often located at the edges, with some portion of the functional groups on the surfaces.[44,45] Our results suggest that either the granular GO has more carboxyl and epoxide functional groups per unit mass or that the size of the granular GO is more amenable to the formation of amide linkages with the CS polymer molecules. The difference in observed N speciation between the two sizes of GO particles may also reflect differences in the GO particle dispersion and aggregation within the CS matrix, where the lower amide speciation of DN-CSGO may indicate GO particle aggregation and a resulting decrease in the accessible surface functional groups available for amide linkage. As a result, the DG-CSGO results in a greater number of interactions between GO and CS, represented by protonated amine and amide groups, than the DN-CSGO composite.

EDX was also used during SEM imaging for the elemental analysis of the membranes and support the results obtained by XPS (Table S1). Fourier transform infrared spectrometry (FTIR) was used as a bulk technique to distinguish chemical bonds present in all of the samples (Figure S4). The FTIR results support the XPS results for both C 1s and N 1s spectra but are not able to resolve the detailed differences identified with XPS.

2.3. Structural Characterization of CSGO Composite Membranes. X-ray diffraction (XRD) characterization (Figure 3) of dry membrane samples was used to evaluate the crystallinity of each of the membranes, as well as the interlayer

DOI: 10.1021/acsomega.7b01266
ACS Omega 2017, 2, 8751–8759

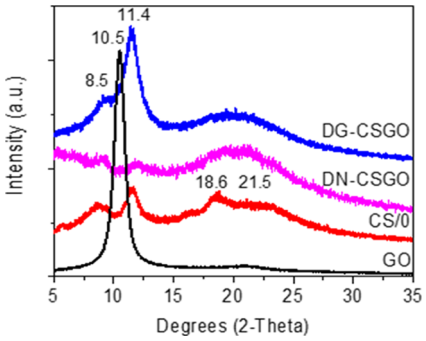

Figure 3. XRD patterns of dry CS/0, GO, and CSGO membranes.

spacing of GO. The XRD pattern of GO shows a sharp peak at 10.5°. The XRD pattern for the CS/0 membrane has two peaks at 8.5 and 11.4°, which are related to the hydrated crystalline structure, and two broad peaks at 18.6 and 21.5°, which are related to the amorphous structure of the CS film. In comparison to the GO membrane, both CSGO membranes result in the loss of the sharp peak at 10.5°, the disappearance of which indicates the exfoliation of GO into the CS matrix. The XRD patterns of the CSGO membranes also show the peaks that are related to CS at 21.5, 18.6, 11.4, and 8.5°. However, the peaks at 18.6 and 21.5° result in significant broadening, suggesting an increase in the structural disorder. Although the incorporation of granular GO particles increases the intensity of the peaks characteristic of CS, the addition of nanoscale GO particles decreases the intensity of these CS-related peaks at 11.4 and 8.5°. The increase in peak intensity of the DG-CSGO pattern at these two peaks suggests an increase in the degree of crystallinity after granular GO addition. However, the intensity reduction for the peak at 11.4° for the DN-CSGO film suggests that this membrane resulted in lower crystallinity after the addition of the nanoscale GO particles to CS. The different results for the DG-CSGO and DN-CSGO membranes again suggest that the GO particle size is in fact a critical parameter for controlling membrane properties, including not only morphology and chemical bonding but also crystallinity. The higher crystallinity of the DG-CSGO is consistent with the layered, ordered cross-sectional morphology observed in Figure 1, as compared to the more disordered, dispersed-particle morphology of the DN-CSGO membrane cross section.

The behavior of the GO and CSGO membranes were also evaluated as wetted membranes by XRD. As shown in Figure S5, the peak of GO membrane is shifted to the left in the wet state due to an increase in the interlayer spacing, whereas no sharp peak was observed for the CSGO membranes in wet state because of loss of crystallinity.

2.4. Membrane Performance: Pure Water Flux and Organic Dye Rejection. The performance of DN-CSGO and DG-CSGO composite membranes were evaluated in a cross-flow cell and challenged with the cationic methylene blue (MB) and anionic methyl orange (MO) dyes. For MB, both composite CSGO membranes were able to remove greater than 95% of MB from the solution at concentrations ranging from 1 to 100 mg/L. The flux rates for these solutions ranged from 2 to 4.5 L/m^2 h with a transmembrane pressure of 344 kPa (3.44 bar), with pure water permeance ranging from 5.8 × 10^{-3} to 0.01 L/m^2 h kPa (0.58−1.3 L/m^2 h bar) (Figure 4). Both DN-CSGO and DG-CSGO membranes resulted in similar thicknesses (Figure S2). Based on the 41 μm thickness obtained from SEM, the hydraulic permeability ranged from 0.24 to 0.54 L μm/m^2 h kPa (24.4−54.1 L μm/m^2 h bar) (Figure S2). The tangential flow on the membrane surface had a cross-flow velocity of 1.8 × 10^{-3} m/s and a Reynolds number of 6.3 × 10^{-5}. The rejection performance of DG-CSGO for MB was quite similar to that of DN-CSGO, with no observable or statistically significant difference in the rejection performance between the two membranes. Further, the rejection performance of the two membranes remained consistent over the range of MB concentrations tested. The water flux decreased at higher MB concentrations for both membranes, and the water flux measured during MB rejection studies was similar to the measured pure water flux (Figure S7). It is perhaps surprising that the membranes behave similarly despite the distinct differences in membrane morphology, structural order, and chemical composition. The similar performance observed may result from the swelling and loss of structural order that occurs in both of the membranes in the hydrated state (as observed in wet membrane XRD, Figure S5b). The loss of order observed in the XRD results also suggests that the differences in nitrogen speciation observed by XPS (Figure 2) are likely lost in the hydrated state, making the two composite membrane structures much more similar in the hydrated state than in the dry state.

In the case of anionic MO, results indicate the importance of electrostatic effects as sorption appears to be the dominant

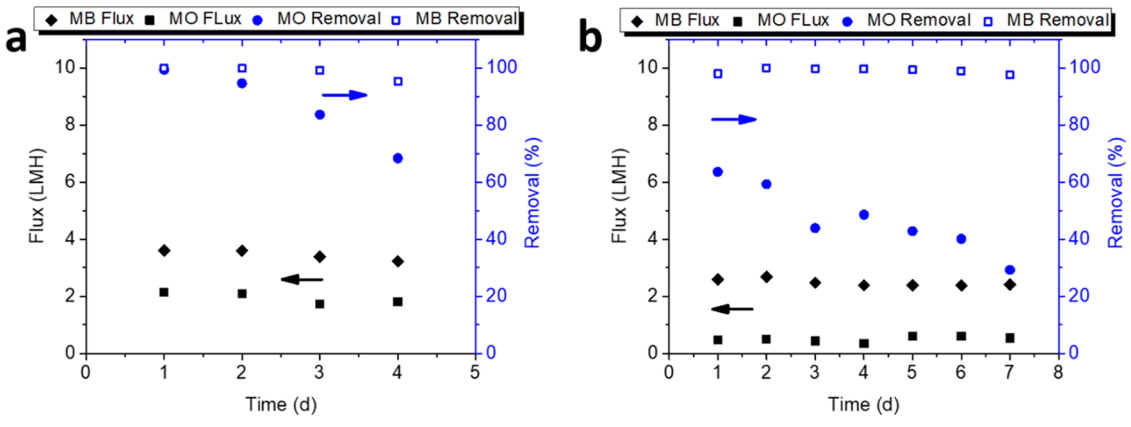

Figure 4. Water flux, MB, and MO removal for (a) DG-CSGO and (b) DN-CSGO composite membranes, 10 mg/L constituent at 344 kPa (3.44 bar), and 1.8 × 10^{-3} m/s cross-flow velocity.

DOI: 10.1021/acsomega.7b01266
ACS Omega 2017, 2, 8751−8759

mechanism of removal with decreased performance over time. It is also noteworthy that in contrast to MB, the performance of GO particle was observed to be dependent on size, with micrometer-scale GO removing 68−99% and the nanometer-scale GO showing modest removal of 29−64%. As the CSGO composite membranes sorbed anionic MO dye, the overall rejection efficiency diminished from 99 to 68% and from 64 to 29% for the DG-CSGO and DN-CSGO membranes, respectively, throughout the duration of evaluation, where the rejection in this case includes both adsorption and physical sieving of the dye. Rejection was observed for the DG-CSGO as the adsorbent sites were occupied; the MO concentration within the concentrate stream initially decreased, but then increased as the experiment continued. For the DN-CSGO, the concentration within the concentrate stream initially decreased and remained constant for the remainder of the experiment, indicating sorption without a clear evidence of rejection. In addition to lower removal efficiency, the flux for MO was also lower than that for MB, with a flux range from 0.5 to 2.1 L/m^2 h, with a transmembrane pressure of 344 kPa (3.44 bar).

Further, although the water flux reported herein is quite low, membrane optimization (i.e., thickness and composition) will likely allow an increase in flux. It is also interesting to note that flux was not increased above the maximum of 4.5 L/m^2 h even when subjected to four different pressures between 1380 and 4140 kPa (13.8−41.4 bar). However, the permeance range of 0.6−1.3 L/m^2 h bar is consistent with the permeance range of 0.5−10 L/m^2 h bar observed for GO composites in the literature where GO is blended within another matrix.[37] Despite the challenges presented for these composite membranes, the initial performance evaluation of MB rejection demonstrates that these membranes hold promise as a material that utilizes the advantageous properties of both CS and GO in a scalable film suitable for roll-to-roll (R2R) manufacturing. The difference in performance between the two dyes analyzed indicates that electrostatic effects, in part, dictate membrane performance. We anticipate this initial proof of concept using CSGO as a competent, scalable membrane for pressure-driven, cross-flow water treatment will serve to guide further optimization of GO mixed matrix membranes.

Of the four types of membranes fabricated, only the composite CSGO membranes were able to be tested in the cross-flow system. The CS/0 membrane was unstable in an aqueous solution, as was expected for an unmodified CS/0 film due to the solubility of chitosan in aqueous solutions. The GO membrane, which was fabricated via the Anodisc-based method vacuum filtration method, was not scalable and did not have a surface area large enough to accommodate the cross-flow cell. The challenges of CS/0 stability and GO fabrication scalability are thus addressed in the formation of the CSGO composite membranes. The robust and scalable CSGO composite membranes were evaluated in the cross-flow system for up to 7 days and resulted in consistent pure water flux measurements. However, in longer flux studies, an increase in pure water flux was observed for some of the membrane samples tested, suggesting an eventual instability of the composite in an aqueous system. This instability is likely due to swelling and loss of structural order; future work on these membranes will necessarily include optimization of membrane stability and evaluation of membrane performance in long-term cross-flow filtration studies.

In all of the experiments, formation of a concentrated MB solution in the reject stream of the cross-flow system (Figure S1d) was indicative of physical rejection. However, both GO and CSGO composite materials are known to be excellent adsorbents for dyes and other contaminants.[18,25,29] Thus, to provide a mechanistic insight and avoid attributing sorption to rejection, a mass balance on the MB was performed (Table 2)

Table 2. Mass Balance of MB Dye in the Feed, Permeate, and Concentrate for DG-CSGO Membranes

pressure (psi)	feed (mg MB)	permeate (mg MB)	concentrate (mg MB)	MB loss (mg)
20	66.8449	0.0017	65.8359	1.0072
50	63.7151	0.0018	64.5282	0[a]
110	61.4986	0.0035	61.9195	0[a]

[a]Concentrate stream contained greater mass of MB than feed, which indicates an analytical error and no observable adsorption.

to demonstrate that the majority of the MB mass was rejected by the CSGO membranes, rather than adsorbed. In parallel, the adsorption capacity of GO and CSGO composite was evaluated. Although GO was measured to adsorb MB with an adsorption capacity, Qe, of 139.29 mg/g, this sorption capacity is greatly diminished to a Qe of 52.40 mg/g for the CSGO composite. The reduction in adsorption capacity is likely due to the interaction between protonated amines of chitosan and oxygen functionalities of GO, which would reduce the number of available surface functional groups that are able to coordinate with MB molecules. This result, along with the mass balance calculations, indicates that as a CSGO composite, sorption is not expected to be a dominant factor, which is a benefit to a membrane separation. Conversely, for MO, sorption appears to be the dominant mechanism, demonstrating the importance of electrostatic effects.

3. CONCLUSIONS

Here, we report on a set of chitosan-graphene oxide composite membranes, where the size of the graphene oxide particles is shown to have a direct impact on the membrane morphology, chemical speciation, structural order, and membrane mechanical properties. CSGO membranes containing either nanometer GO or micrometer-scale GO result in similar filtration performance when pure water flux and rejection of the cationic dye methylene blue. However, the differences in rejection and flux observed during the filtration of anionic dye methyl orange suggest the size of GO may impact the filtration performance and that the properties of the contaminant are important to understand in relation to the properties of the composite membranes. Overall, the CSGO membranes had rejections of at least 95% for cationic methylene blue (MB), with the mass balances obtained from measurements of the feed, concentrate, and permeate. This result suggests the dominant mechanism of removal is the physical rejection for both GO particle sizes. For anionic methyl orange (MO), the results indicate sorption as the dominant mechanism of removal, and performance is dependent on both GO particle size and time, with micrometer-scale GO removing 68−99% and nanometer-scale GO showing modest removal of 29−64%. The pure water flux for CSGO composite membranes ranged from 2 to 4.5 L/m^2 h at a transmembrane pressure of 344 kPa (3.44 bar), with pure water permeance ranging from 5.8×10^{-3} to 0.01 L/m^2 h kPa (0.58−1.3 L/m^2 h bar).

DOI: 10.1021/acsomega.7b01266
ACS Omega 2017, 2, 8751−8759

4. MATERIALS AND METHODS

4.1. Materials. Graphene oxide was used in the dry solid and water-dispersed state. GO was obtained commercially as an aqueous suspension with a concentration of 6.2 g/L (Graphene Supermarket, Calverton, NY). Granular and nanoscale dry solids GO samples were also obtained at two different commercially reported particle sizes (granular, around 90% 0.3−0.7 μm and nanoscale, around 90% 80−105 nm, Graphene Supermarket, Calverton, NY). The chitosan used was a form of deacetylated chitin from Sigma-Aldrich (medium molecular weight (MW), poly-D-glucosamine). Acetic acid was obtained from Sigma-Aldrich (≥99%). Methylene blue (MB) was used as a cationic molecular probe for this study and has a molecular weight (MW) of 319.85 g/mol and a density of 1.77 g/mL. Methyl orange (MO) (MW = 327.33 g/mol) was used as an anionic molecular probe. Solutions of MB and MO were prepared from the laboratory grade powder obtained from Merck and Fisher Scientific, respectively. Millipore nitrocellulose membranes from Bio-Rad (Hercules, CA) (Roll, 0.45 μm, 30 cm × 3.5 m, Cat #: 1620115) were used for the mechanical support during cross-flow filtration. Anopore Anodized Aluminum Oxide Anodiscs were obtained from Whatman GE Healthcare Life Sciences (0.2 μm pore size, 60 μm thick, 47 mm diameter) and used for vacuum filtration of GO suspensions.

4.2. Preparation of Graphene Oxide (GO) Membranes. To prepare GO membranes, 50 mL GO suspensions were prepared by diluting the commercial GO suspension (6.2 g/L) to 1 g/L with purified water. The suspension was sonicated for 1 h and placed on a porous anodized aluminum oxide (AAO) filter for vacuum filtration.[38] The pH of the suspension was ∼3 due to residual acid content from graphene oxidation. Filtration of the suspension took approximately 72 h, at which point the dissolution of Al^{3+} from the AAO filter provided a cross-linking agent for the GO laminate membrane to form the GO flakes assembled on the AAO filter.

4.3. Preparation of Chitosan Membranes (CS/0). To prepare CS/0 membranes, 500 mg of medium molecular weight CS was added to a 100 mL Nalgene bottle containing 50 mL water and approximately 0.33 mL 99% acetic acid. This procedure was followed by stirring the solution for 72 h. Finally, the solution was poured into a petri dish and dried in an incubator for 48 h.

4.4. Preparation of Chitosan-Graphene Oxide (CSGO) Membranes. A CS-rich GO suspension was prepared as follows: 0.3013 g of GO powder was added to 100 mL of purified water, stirred for 15 min, and sonicated for 30 min. The dispersion was then poured into an Erlenmeyer flask with 1.5 g of CS and 1 mL of acetic acid (1% acetic acid solution). The composition of this casting solution was 1.5 wt % CS and 0.3 wt % GO, and the CS/GO ratio in the cast membrane was 5:1 w/w. This dispersion was placed on a stir plate and stirred for 3 days at the highest speed. The mixing caused the CS powder to fully dissolve and the GO to disperse in the aqueous acetic acid solution and form a uniform mixture with a metallic gray color. The CSGO membranes were fabricated by evaporation under reduced pressure for 72 h, which eliminated the need for the AAO filter support used for GO-only membranes.

4.5. Morphological and Chemical Analysis. Surface and cross-sectional membrane morphologies were evaluated by scanning electron microscopy (SEM, Nova Nanolab 200, 15 kV). For cross-sectional observation, liquid nitrogen was used to freeze the samples before fracturing; the membranes were then freeze-fractured so that the membrane cross section was exposed. Membrane sections were mounted onto the SEM stubs with the top surface, bottom surface, or cross section oriented for imaging. The films were sputter coated with gold to prevent charging and then analyzed by SEM. Attenuated total reflectance Fourier transform infrared spectrometry (ATR-FTIR) (Spectrum BX FTIR spectrophotometer equipped with Pike ATR accessory) was used to evaluate the molecular interactions between GO and CS. The spectra were obtained at 8 cm^{-1} resolution in the absorbance wavelength range of 4000−500 cm^{-1}. X-ray photoelectron spectroscopy (XPS; PHI Versaprobe 5000 with PHI MultiPack data analysis software) was used to evaluate the chemical composition of the films. Initial survey scans (0−1400 eV binding energy) were followed by detailed scans for carbon (275−295 eV) and nitrogen (390−410 eV). High-resolution X-ray diffraction (XRD, Philips X'Pert- MRD diffractometer, Cu Kα radiation source) was used to determine the crystallinity of the samples. The XRD patterns were taken within the recorded region of 2θ from 5 to 35°, with a scanning speed of 1 min^{-1} at a voltage of 45.0 kV and a current of 40.0 mA.

4.6. Tensile Strength Testing. To measure the mechanical properties of the CS/0 and CSGO membranes, a universal mechanical testing machine (Instron 5944) was used to obtain the stress−strain curves. The samples were cut in the same shape (40 mm × 10 mm) with a different thickness, which was measured by the cross-sectional SEM images (Figure S2). Five replicates were performed for each membrane at room temperature with a strain rate 5.0 mm/min and 0.05 N preload.

4.7. Membrane Filtration and Rejection Experiments. *4.7.1. Cross-Flow Setup.* After fabrication, the freestanding membranes were sectioned with a Sterlitech membrane die and placed one at a time in a cross-flow membrane cell to evaluate pure water flux and contaminant rejection. The cross-flow system (Figure S1e) was set up such that the cell concentrate was recycled to the feed flask; this was done so that the cross-flow cell could run over several days with the same feed solution. Samples from the concentrate and permeate streams were collected at least once every 24 h to determine the flux and rejection. System and transmembrane pressure data were recorded via pressure transducers obtained from OMEGA Engineering. To control potential swelling of the membranes, the membrane was physically confined between two nitrocellulose microfiltration membranes (0.45 μm pore size, 30 cm × 3.5 m) during the cross-flow filtration. Control experiments were performed to confirm that when coupled with the CSGO membranes, the nitrocellulose support would not contribute to dye removal. Adsorptive removal with the nitrocellulose was less than 1% and was solely used as structural support for positive pressure tangential flow experiments.

4.7.2. Organic Dye Analysis. CSGO membranes were tested for their ability to remove MB and MO in a series of cross-flow filtration experiments. Dye solution, at varying concentrations, was flowed through the cross-flow cell at pressures ranging from 69 to 414 kPa. The initial and final concentrations for the concentrate and permeate were analyzed using an Agilent 8453 UV−vis spectrophotometer. A linear calibration curve was used to calculate the MB and MO concentrations from the absorbance readings, and the MB and MO detection limits were estimated at 0.005 and 0.1 mg/L, respectively.

DOI: 10.1021/acsomega.7b01266
ACS Omega 2017, 2, 8751−8759

■ ASSOCIATED CONTENT

Supporting Information

The Supporting Information is available free of charge on the ACS Publications website at DOI: 10.1021/acsomega.7b01266.

Images and schematic of cross-flow filtration setup; membrane thickness measurements; XPS results for aluminum; EDX, XPS, FTIR, SEM, AFM, and XRD characterization data for GO; XRD results for dry and wet membranes; tensile test results; and additional water flux data (PDF)

■ AUTHOR INFORMATION

Corresponding Author

*E-mail: greenlee@uark.edu. Phone: 4987-575-5976. Fax: 479-575-7926.

ORCID

Lauren F. Greenlee: 0000-0001-6147-1533

Notes

The authors declare no competing financial interest.

■ ACKNOWLEDGMENTS

We acknowledge the Institute for Nanoscience and Engineering at the University of Arkansas for facilitating and supporting membrane characterization and data analysis. We acknowledge Prof. Kartik Balachandran and his research group at the University of Arkansas for help with tensile testing of the membranes. Funding for membrane fabrication and cross-flow filtration testing was provided by the U.S. Army Environmental Quality and Installations Research Program (Dr. E. Ferguson, Technical Director).

■ REFERENCES

(1) Šostar-Turk, S.; Petrinić, I.; Simonič, M. Laundry wastewater treatment using coagulation and membrane filtration. *Resour., Conserv. Recycl.* **2005**, *44*, 185−196.

(2) Qu, X.; Alvarez, P. J. J.; Li, Q. Applications of nanotechnology in water and wastewater treatment. *Water Res.* **2013**, *47*, 3931−3946.

(3) Greenlee, L. F.; Lawler, D. F.; Freeman, B. D.; Marrot, B.; Moulin, P. Reverse osmosis desalination: Water sources, technology, and today's challenges. *Water Res.* **2009**, *43*, 2317−2348.

(4) Mahmoudi, N.; Reed, L.; Moix, A.; Alshammari, N.; Hestekin, J.; Servoss, S. L. PEG-mimetic peptoid reduces protein fouling of polysulfone hollow fibers. *Colloids Surf., B* **2017**, *149*, 23−29.

(5) Jin, F.; Lv, W.; Zhang, C.; Li, Z.; Su, R.; Qi, W.; Yang, Q.-H.; He, Z. High-performance ultrafiltration membranes based on polyethersulfone−graphene oxide composites. *RSC Adv.* **2013**, *3*, 21394−21397.

(6) Chang, X.; Wang, Z.; Quan, S.; Xu, Y.; Jiang, Z.; Shao, L. Exploring the synergetic effects of graphene oxide (GO) and polyvinylpyrrodione (PVP) on poly (vinylylidenefluoride)(PVDF) ultrafiltration membrane performance. *Appl. Surf. Sci.* **2014**, *316*, 537−548.

(7) Aghajani, M.; Maruf, S. H.; Wang, M.; Yoshimura, J.; Pichorim, G.; Greenberg, A.; Ding, Y. Relationship between permeation and deformation for porous membranes. *J. Membr. Sci.* **2017**, *526*, 293−300.

(8) Shao, L.; Cheng, X.; Wang, Z.; Ma, J.; Guo, Z. Tuning the performance of polypyrrole-based solvent-resistant composite nanofiltration membranes by optimizing polymerization conditions and incorporating graphene oxide. *J. Membr. Sci.* **2014**, *452*, 82−89.

(9) Yang, M.; Zhao, C.; Zhang, S.; Li, P.; Hou, D. Preparation of graphene oxide modified poly (m-phenylene isophthalamide) nanofiltration membrane with improved water flux and antifouling property. *Appl. Surf. Sci.* **2017**, *394*, 149−159.

(10) Yin, J.; Zhu, G.; Deng, B. Graphene oxide (GO) enhanced polyamide (PA) thin-film nanocomposite (TFN) membrane for water purification. *Desalination* **2016**, *379*, 93−101.

(11) Vaseghi, G.; Ghassemi, A.; Loya, J. Characterization of reverse osmosis and nanofiltration membranes: effects of operating conditions and specific ion rejection. *Desalin. Water Treat.* **2016**, *57*, 23461−23472.

(12) Çulfaz, P. Z.; Haddad, M.; Wessling, M.; Lammertink, R. G. Fouling behavior of microstructured hollow fibers in cross-flow filtrations: critical flux determination and direct visual observation of particle deposition. *J. Membr. Sci.* **2011**, *372*, 210−218.

(13) Shao, L.; Chang, X.; Zhang, Y.; Huang, Y.; Yao, Y.; Guo, Z. Graphene oxide cross-linked chitosan nanocomposite membrane. *Appl. Surf. Sci.* **2013**, *280*, 989−992.

(14) Travlou, N. A.; Kyzas, G. Z.; Lazaridis, N. K.; Deliyanni, E. A. Graphite oxide/chitosan composite for reactive dye removal. *Chem. Eng. J.* **2013**, *217*, 256−265.

(15) Carson, L.; Kelly-Brown, C.; Stewart, M.; Oki, A.; Regisford, G.; Luo, Z.; Bakhmutov, V. I. Synthesis and characterization of chitosan−carbon nanotube composites. *Mater. Lett.* **2009**, *63*, 617−620.

(16) Pan, Y.; Wu, T.; Bao, H.; Li, L. Green fabrication of chitosan films reinforced with parallel aligned graphene oxide. *Carbohydr. Polym.* **2011**, *83*, 1908−1915.

(17) He, L.; Wang, H.; Xia, G.; Sun, J.; Song, R. Chitosan/graphene oxide nanocomposite films with enhanced interfacial interaction and their electrochemical applications. *Appl. Surf. Sci.* **2014**, *314*, 510−515.

(18) Ramesha, G. K.; Kumara, A. V.; Muralidhara, H.; Sampath, S. Graphene and graphene oxide as effective adsorbents toward anionic and cationic dyes. *J. Colloid Interface Sci.* **2011**, *361*, 270−277.

(19) Kim, F.; Cote, L. J.; Huang, J. Graphene Oxide: Surface Activity and Two-Dimensional Assembly. *Adv. Mater.* **2010**, *22*, 1954−1958.

(20) Kim, J.; Cote, L. J.; Kim, F.; Yuan, W.; Shull, K. R.; Huang, J. Graphene oxide sheets at interfaces. *J. Am. Chem. Soc.* **2010**, *132*, 8180−8186.

(21) Chandra, V.; Park, J.; Chun, Y.; Lee, J. W.; Hwang, I.-C.; Kim, K. S. Water-dispersible magnetite-reduced graphene oxide composites for arsenic removal. *ACS Nano* **2010**, *4*, 3979−3986.

(22) Zhang, W.; Zhou, C.; Zhou, W.; Lei, A.; Zhang, Q.; Wan, Q.; Zou, B. Fast and considerable adsorption of methylene blue dye onto graphene oxide. *Bull. Environ. Contam. Toxicol.* **2011**, *87*, 86−90.

(23) Griggs, C. S.; Medina, V. F. Graphene and Graphene Oxide Membranes for Water Treatment. *McGraw Hill Yearbook of Science and Technology*; McGraw-Hill Education, 2016.

(24) Rezaee, R.; Nasseri, S.; Mahvi, A. H.; Nabizadeh, R.; Mousavi, S. A.; Rashidi, A.; Jafari, A.; Nazmara, S. Fabrication and characterization of a polysulfone-graphene oxide nanocomposite membrane for arsenate rejection from water. *J. Environ. Health Sci. Eng.* **2015**, *13*, 61.

(25) He, Y. Q.; Zhang, N. N.; Wang, X. D. Adsorption of graphene oxide/chitosan porous materials for metal ions. *Chin. Chem. Lett.* **2011**, *22*, 859−862.

(26) Bao, H.; Pan, Y.; Ping, Y.; Sahoo, N. G.; Wu, T.; Li, L.; Li, J.; Gan, L. H. Chitosan-functionalized graphene oxide as a nanocarrier for drug and gene delivery. *Small* **2011**, *7*, 1569−1578.

(27) Justin, R.; Chen, B. Characterisation and drug release performance of biodegradable chitosan−graphene oxide nanocomposites. *Carbohydr. Polym.* **2014**, *103*, 70−80.

(28) Yang, X.; Tu, Y.; Li, L.; Shang, S.; Tao, X.-m. Well-Dispersed Chitosan/Graphene Oxide Nanocomposites. *ACS Appl. Mater. Interfaces* **2010**, *2*, 1707−1713.

(29) Chen, Y.; Chen, L.; Bai, H.; Li, L. Graphene oxide−chitosan composite hydrogels as broad-spectrum adsorbents for water purification. *J. Mater. Chem. A* **2013**, *1*, 1992−2001.

(30) Zuo, P.-P.; Feng, H.-F.; Xu, Z.-Z.; Zhang, L.-F.; Zhang, Y.-L.; Xia, W.; Zhang, W.-Q. Fabrication of biocompatible and mechanically reinforced graphene oxide-chitosan nanocomposite films. *Chem. Cent. J.* **2013**, *7*, 39.

(31) Fan, H.; Wang, L.; Zhao, K.; Li, N.; Shi, Z.; Ge, Z.; Jin, Z. Fabrication, mechanical properties, and biocompatibility of graphene-

DOI: 10.1021/acsomega.7b01266
ACS Omega 2017, 2, 8751−8759

reinforced chitosan composites. *Biomacromolecules* **2010**, *11*, 2345−2351.
(32) Wang, T.; Zhang, S.; Mao, C.; Song, J.; Niu, H.; Jin, B.; Tian, Y. Enhanced electrochemiluminescence of CdSe quantum dots composited with graphene oxide and chitosan for sensitive sensor. *Biosens. Bioelectron.* **2012**, *31*, 369−375.
(33) Singh, A.; Sinsinbar, G.; Choudhary, M.; Kumar, V.; Pasricha, R.; Verma, H.; Singh, S. P.; Arora, K. Graphene oxide-chitosan nanocomposite based electrochemical DNA biosensor for detection of typhoid. *Sens. Actuators, B* **2013**, *185*, 675−684.
(34) Li, L.; Fan, L.; Sun, M.; Qiu, H.; Li, X.; Duan, H.; Luo, C. Adsorbent for chromium removal based on graphene oxide functionalized with magnetic cyclodextrin−chitosan. *Colloids Surf., B* **2013**, *107*, 76−83.
(35) Yu, B.; Xu, J.; Liu, J.-H.; Yang, S.-T.; Luo, J.; Zhou, Q.; Wan, J.; Liao, R.; Wang, H.; Liu, Y. Adsorption behavior of copper ions on graphene oxide−chitosan aerogel. *J. Environ. Chem. Eng.* **2013**, *1*, 1044−1050.
(36) Fan, L.; Luo, C.; Sun, M.; Li, X.; Qiu, H. Highly selective adsorption of lead ions by water-dispersible magnetic chitosan/graphene oxide composites. *Colloids Surf., B* **2013**, *103*, 523−529.
(37) Amadei, C. A.; Vecitis, C. D. How to Increase the Signal-to-Noise Ratio of Graphene Oxide Membrane Research. *J. Phys. Chem. Lett.* **2016**, *7*, 3791−3797.
(38) Dikin, D. A.; Stankovich, S.; Zimney, E. J.; Piner, R. D.; Dommett, G. H.; Evmenenko, G.; Nguyen, S. T.; Ruoff, R. S. Preparation and characterization of graphene oxide paper. *Nature* **2007**, *448*, 457−460.
(39) Yeh, C.-N.; Raidongia, K.; Shao, J.; Yang, Q.-H.; Huang, J. On the origin of the stability of graphene oxide membranes in water. *Nat. Chem.* **2015**, *7*, 166−170.
(40) Park, S.; Dikin, D. A.; Nguyen, S. T.; Ruoff, R. S. Graphene oxide sheets chemically cross-linked by polyallylamine. *J. Phys. Chem. C* **2009**, *113*, 15801−15804.
(41) Sobon, G.; Sotor, J.; Jagiello, J.; Kozinski, R.; Zdrojek, M.; Holdynski, M.; Paletko, P.; Boguslawski, J.; Lipinska, L.; Abramski, K. M. Graphene oxide vs. reduced graphene oxide as saturable absorbers for Er-doped passively mode-locked fiber laser. *Opt. Express* **2012**, *20*, 19463−19473.
(42) Han, D.; Yan, L.; Chen, W.; Li, W. Preparation of chitosan/graphene oxide composite film with enhanced mechanical strength in the wet state. *Carbohydr. Polym.* **2011**, *83*, 653−658.
(43) Compton, O. C.; Dikin, D. A.; Putz, K. W.; Brinson, L. C.; Nguyen, S. T. Electrically conductive "alkylated" graphene paper via chemical reduction of amine-functionalized graphene oxide paper. *Adv. Mater.* **2010**, *22*, 892−896.
(44) Sun, P.; Zheng, F.; Zhu, M.; Song, Z.; Wang, K.; Zhong, M.; Wu, D.; Little, R. B.; Xu, Z.; Zhu, H. Selective Trans-Membrane Transport of Alkali and Alkaline Earth Cations through Graphene Oxide Membranes Based on Cation−π Interactions. *ACS Nano* **2014**, *8*, 850−859.
(45) Sun, P.; Zhu, M.; Wang, K.; Zhong, M.; Wei, J.; Wu, D.; Xu, Z.; Zhu, H. Selective Ion Penetration of Graphene Oxide Membranes. *ACS Nano* **2013**, *7*, 428−437.

DOI: 10.1021/acsomega.7b01266
ACS Omega 2017, 2, 8751−8759